



OPEN

## Multi-spectroscopic, thermodynamic, and molecular docking/dynamic approaches for characterization of the binding interaction between calf thymus DNA and palbociclib

Galal Magdy<sup>1✉</sup>, Moataz A. Shaldam<sup>2</sup>, Fathalla Belal<sup>3</sup> & Heba Elmansi<sup>3</sup>

Studying the binding interaction between biological macromolecules and small molecules has formed the core of different research aspects. The interaction of palbociclib with calf thymus DNA at simulated physiological conditions (pH 7.4) was studied using different approaches, including spectrophotometry, spectrofluorimetry, FT-IR spectroscopy, viscosity measurements, ionic strength measurements, thermodynamic, molecular dynamic simulation, and docking studies. The obtained findings showed an apparent binding interaction between palbociclib and calf thymus DNA. Groove binding mode was confirmed from the findings of competitive binding studies with ethidium bromide or rhodamine B, UV-Vis spectrophotometry, and viscosity assessment. The binding constant ( $K_b$ ) at 298 K calculated from the Benesi–Hildebrand equation was found to be  $6.42 \times 10^3 \text{ M}^{-1}$ . The enthalpy and entropy changes ( $\Delta H^0$  and  $\Delta S^0$ ) were  $-33.09 \text{ kJ mol}^{-1}$  and  $61.78 \text{ J mol}^{-1} \text{ K}^{-1}$ , respectively, showing that hydrophobic and hydrogen bonds constitute the primary binding forces. As indicated by the molecular docking results, palbociclib fits into the AT-rich region of the B-DNA minor groove with four base pairs long binding site. The dynamic performance and stability of the formed complex were also evaluated using molecular dynamic simulation studies. The in vitro study of the intermolecular binding interaction of palbociclib with calf thymus DNA could guide future clinical and pharmacological studies for the rational drug scheming with enhanced or more selective activity and greater efficacy.

Palbociclib (PLB) is 6-acetyl-8-cyclopentyl-5-methyl-2-[(5-piperazin-1-yl)pyridin-2-yl]amino]pyrido[2,3-d]pyrimidin-7-one<sup>1</sup> (Fig. 1). It is an anti-cancer drug indicated for breast cancer under the trade name: Ibrance<sup>®</sup> capsules. The capsules are present in different concentrations: 75, 100, and 125 mg as a free base<sup>2</sup>. PLB is used in combination with other drugs to treat hormone receptor-positive, advanced breast cancer (breast cancer that grows in response to hormones such as estrogen) or breast cancer that has spread to other parts of the body in women who have gone through menopause (the end of monthly menstrual periods). It is also used to treat breast cancer that has spread to other body regions in persons treated with antiestrogen drugs like tamoxifen. It has been considered by FDA to treat postmenopausal ER-positive/HER2-negative advanced breast cancer with letrozole as first-line therapy<sup>3</sup>. PLB belongs to the kinase inhibitor family of drugs. It functions by obstructing the action of the abnormal protein that signals cancer cells to multiply, which aids in preventing or slowing cancer cell spread<sup>4</sup>. As breast cancer is generally the second most common cancer and the most common cancer in women<sup>5</sup>, there is great importance for studying PLB molecular binding interaction with calf thymus DNA (CT-DNA) to get a clearer vision of its mechanism of action and pharmacological effect.

DNA draws out an essential role in life as it directs the biosynthesis of enzymes and proteins in a living cell by the replication and transcription of genetic information. It is, therefore, a vital carrier for this information. The

<sup>1</sup>Pharmaceutical Analytical Chemistry Department, Faculty of Pharmacy, Kafrelsheikh University, P.O. Box 33511, Kafrelsheikh, Egypt. <sup>2</sup>Pharmaceutical Chemistry Department, Faculty of Pharmacy, Kafrelsheikh University, P.O. Box 33511, Kafrelsheikh, Egypt. <sup>3</sup>Pharmaceutical Analytical Chemistry Department, Faculty of Pharmacy, Mansoura University, P.O. Box 35516, Mansoura, Egypt. ✉email: galal\_magdy@pharm.kfs.edu.eg

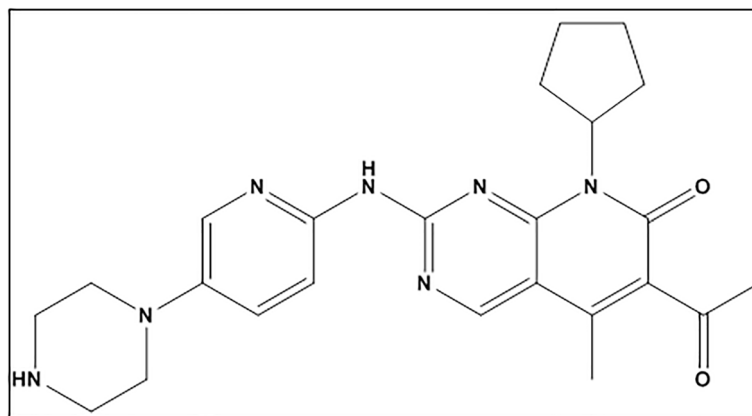


**Figure 1.** Chemical structure of PLB.

interaction of small ligand molecules with DNA and other macromolecules gives an indication for drug design and synthesis or improvement of drugs with better selectivity and efficacy<sup>6–20</sup>.

Drugs can react with DNA through non-covalent or covalent bonds. Usually, the non-covalent pattern is predominant<sup>21,22</sup>. Different sites in the DNA molecule are susceptible to binding as follows: (1) in the minor groove, (2) in the major groove, (3) between two base pairs (full intercalation), (4) on the outside of the helix, and (5) electrostatic binding<sup>23</sup>. Usually, no single method can provide a complete vision for drug-DNA interaction. Therefore, it is essential to provide rapid, high throughput, continuous, and economical techniques for the assessment of the interaction of DNA with different drugs so as to help in drug discovery and approval processes.

From the literature, the *in vitro* binding interaction between PLB and CT-DNA was not reported, and the current work introduces the first study for exploring the binding interaction between PLB and CT-DNA, giving detailed information about the nature of this interaction including binding mode, binding constant, specific binding site, and interaction forces. Consequently, the current study aimed to conduct a comprehensive investigation of the interaction of PLB with CT-DNA employing a variety of approaches, including UV-visible spectrophotometry, spectrofluorimetry, FT-IR spectroscopy, viscosity measurements, and ionic strength measurements. Additionally, thermodynamic, molecular dynamic simulation, and molecular docking studies were also accomplished further to clarify binding mode, forces, and sites. Although PLB is an FDA-approved cyclin-dependent kinase inhibitor, the *in vitro* study of its intermolecular binding interaction with CT-DNA could provide guidance for future clinical and pharmacological studies for the rational drug scheming with enhanced or more selective activity and greater efficacy.

## Experimental

**Materials and chemicals.** Palbociclib was kindly provided by Pfizer, Freiburg, Germany. PLB's stock solution was prepared in methanol with a final concentration of  $1.0 \times 10^{-3}$  M. CT-DNA, Tris-HCl, ethidium bromide (EB), and Rhodamine B (RB) were purchased from Sigma Aldrich (St. Louis, MO, USA). The chemicals used throughout this study were of analytical grade.

Tris-HCl buffer solution (0.05 M) was prepared in distilled water, and its pH was set at 7.4 in all experiments. Additionally, CT-DNA stock solution was obtained by dissolving in Tris-HCl buffer with frequent stirring to obtain a homogenous solution. CT-DNA solution's purity was assessed by computing the absorbance ratio of  $A_{260}/A_{280}$ , which was found to be 1.903 (over 1.8), confirming that there is no protein contamination in CT-DNA<sup>24–27</sup>. The final concentration of CT-DNA solution was measured using the extinction coefficient of  $6600 \text{ M}^{-1} \text{ cm}^{-1}$  of a single nucleotide at 260 nm ( $T = 298 \text{ K}$ )<sup>28–30</sup>. The prepared CT-DNA solutions were kept at 4 °C and utilized within five days. Each of EB and RB ( $1.0 \times 10^{-3}$  M) was prepared by dissolving in ethanol as they suffer from low water solubility and also stored at 4 °C.

## Instrumentation.

- T80+ UV/VIS PC Spectrophotometer (PG Instruments Ltd., Woodway Lane, Wibtoft, England) with a 1.0 cm quartz cell was used for the spectrophotometric measurements.
- Agilent Technologies Cary Eclipse spectrofluorimeter with Xenon flash lamp (Santa Clara, CA 95051, USA) was used for the spectrofluorimetric measurements.
- Oswald Viscometer, at a controlled temperature of 298 K, was also used. The capillary's inner diameter was 0.57 mm.

**Study of PLB-CT-DNA interaction.** *Spectrophotometric measurements.* The UV spectra of  $8.25 \times 10^{-5}$  M CT-DNA solutions were scanned from 200 to 400 nm upon adding increased concentrations of PLB in the range of ( $0$ – $2.5 \times 10^{-5}$  M) at four distinct temperatures (298, 303, 308, and 313 K) in order to estimate the binding con-

DNA (PDB ID)	Sequence	Grid points (coordinates/sizes)
3EY0	5'-(ATATATATAT)-3'	(16.394, 10.415, 90.220)/(80, 60, 60)
1D29	5'-(CGTGAATTCACG)-3'	(14.920, 20.905, 8.820)/(60, 60, 110)
1BNA	5'-(CGCGAATTCGCG)-3'	(14.780, 20.976, 8.807)/(60, 60, 110)

**Table 1.** PDB entries and grid point data for the three DNA sequences used for the molecular docking study.

stants and evaluate the temperature effect on the drug-CT-DNA interaction. The corresponding PLB solutions served as references. Furthermore, the absorbance value of a mixed solution of PLB ( $2.0 \times 10^{-5}$  M) and CT-DNA ( $82.5 \times 10^{-5}$  M) was examined at 298 K, varying the NaCl concentration from 0 to 0.07 M to evaluate the effect of ionic strength.

**Spectrofluorimetric measurements.** In the presence and absence of different PLB concentrations, fluorescence emission spectra were recorded for mixtures of CT-DNA (57.0  $\mu$ M) with fluorescent probes; RB (4.0  $\mu$ M) and EB (2.0  $\mu$ M) corresponding to groove and intercalation binding probes, respectively. Excitation wavelengths for RB and EB were adjusted at 465 and 525 nm, with emission spectra obtained at 576 and 574 nm, respectively. All spectra were measured three times, and the average was calculated with a blank experiment conducted similarly.

**Viscosity measurements.** A viscosity study was performed at 298 K using increasing concentrations of PLB ( $0-2.5 \times 10^{-5}$  M), whereas the CT-DNA concentration in Tris-HCl solution was maintained at  $8.25 \times 10^{-5}$  M. The flow times of the CT-DNA solutions were recorded using a digital stopwatch. An average of 3 determinations was recorded. The viscosity was calculated by referring to the formula ( $\eta = (t - t_0)/t_0$ ), where ( $t$ ) represents the measured flow times of CT-DNA-containing solutions and ( $t_0$ ) represents the flow time of Tris-HCl buffer alone. The average readings were utilized to determine the relative specific viscosity ( $(\eta/\eta_0)^{1/3}$ ), where  $\eta$  and  $\eta_0$  are the CT-DNA specific viscosities in the presence and absence of PLB, respectively<sup>13,26</sup>. The results were represented as  $(\eta/\eta_0)^{1/3}$  against the binding ratio  $r$  ( $r = [\text{PLB}]/[\text{CT-DNA}]$ ).

**FT-IR spectroscopy.** The Fourier Transform Infrared (FT-IR) spectra were recorded using ThermoFisher Scientific Nicolet-iS10 FT-IR Spectrometer, from Thermo Fisher Scientific (168 Third Avenue Waltham, MA, USA). It was equipped with a Ge/KBr beam splitter and a DTGS (deuterated triglycine sulfate) detector. Spectra were recorded as 100 scans with a resolution of  $4 \text{ cm}^{-1}$  from 4000 to  $500 \text{ cm}^{-1}$ . PLB with CT-DNA samples were incubated for 2 h. The spectra of CT-DNA alone and PLB-CT-DNA complexes were recorded and subtracted from the background spectra<sup>31,32</sup>. A constant concentration of CT-DNA was used (14.0 mM) while a set of solutions containing different PLB concentrations were prepared, maintaining the ratios of PLB:CT-DNA at 1:10, 1:20, 1:50, and 1:100<sup>32</sup>.

**Molecular docking.** Docking studies were accomplished to explore the binding modes of PLB to three B-DNA sequences using AutoDock 4.2<sup>33</sup>. The 3D coordinates of three B-DNA sequences (1D29<sup>34</sup>, 3EY0<sup>35</sup>, and 1BNA<sup>36</sup>) were retrieved from Protein Data Bank (PDB) and were prepared using the Kollman approach<sup>37</sup>, which included adding partial atomic charges to DNA sequences. The PubChem Database<sup>1</sup> was used to obtain the PLB structure, and energy was minimized using Gaussian 03 software by density functional theory (DFT) at UB3lyp/6-311 + g(d) level till the eigenvalue of the Hessian matrix was positive. The genetic algorithm was utilized for energy evaluation as a search method with a population size of 100 and 2.5 million times. Table 1 specifies the grid box used for each DNA helix at a spacing point of 0.375. The 3D visualization and 2D schematic presentation for DNA-PLB complexes were generated by Chimera 1.13<sup>38</sup> and LigPlot<sup>+</sup> V1.4.5 software<sup>39</sup>, respectively.

**Molecular dynamic simulation.** The DNA-PLB complex (3EY0) generated from the docking studies was constituted before simulation by adding hydrogen, optimizing, and solvating the complex using VMD 1.9<sup>40</sup>. DNA-PLB complex (3EY0) was placed in Periodic Boundary Conditions (PBC) water box and neutralized with NaCl (0.15 M). In this study, two molecular dynamic (MD) simulations were carried out, one for free DNA sequence (3EY0) and the other for PLB-associated DNA sequence. The MD simulation was carried out following the simulation parameters given in the literature<sup>41</sup>. Both MD simulations were executed for 50 ns using NAMD 2.13<sup>42</sup> employing CHARMM36 force-field parameters<sup>43</sup>.

## Results and discussion

**Determination of binding mode of PLB with CT-DNA.** **Spectrophotometric measurements.** This approach is based on observing the alteration in the location and intensity of CT-DNA distinctive absorption bands at 260 nm, that are linked to the  $\pi-\pi^*$  transition of DNA's base pairs<sup>13,26</sup>. It was observed that the intensity of the CT-DNA solution increased gradually upon the increment in the concentration of PLB, as illustrated in Fig. 2A, while the peak location remained almost unchanged. Accordingly, the binding manner of PLB with CT-DNA is suggested to be groove binding instead of intercalation, according to the shift rule for DNA's distinctive absorption peak<sup>26,44,45</sup>. The complex formation was further confirmed by non-overlapping of the absorption spectrum of PLB, CT-DNA, and the difference spectrum (Fig. 2B)<sup>15,19</sup>.

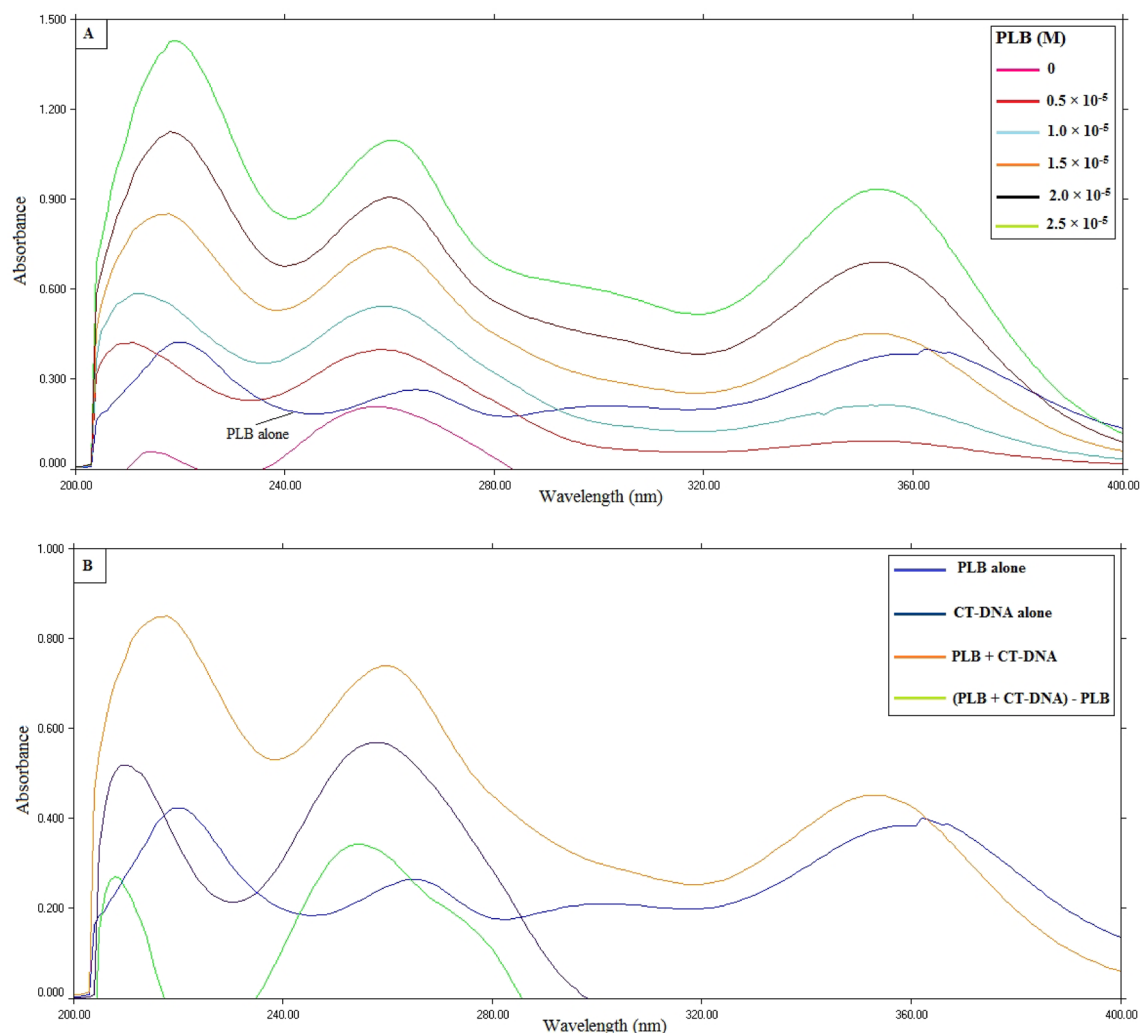


**Figure 2.** UV absorption spectra of (A) CT-DNA ( $8.25 \times 10^{-5}$  M) titrated with increasing concentrations of PLB ( $0$ – $2.5 \times 10^{-5}$  M), (B) PLB alone, CT-DNA alone, PLB-CT-DNA complex, and the difference spectrum.

**Viscosity measurements.** Viscosity measurements are highly sensitive to the variations in the DNA length<sup>46</sup>. The conventional intercalative binding mechanism has been observed to considerably alter the DNA solution viscosity as it needs a large and adequate space between consecutive base pairs to extend the double helix and provide accommodation for micro-molecules. Furthermore, a molecule's non-classical intercalation may cause the DNA helix to twist, lowering its length and viscosity. On the other hand, electrostatic and groove binding mechanisms have little to no effect on DNA viscosity<sup>13,45–48</sup>. The relative specific viscosity  $(\eta/\eta^0)^{1/3}$  of CT-DNA was found to be practically constant, as shown in Fig. 3, confirming PLB groove binding with CT-DNA, which is compatible with the spectrophotometric study findings.

**Assessment of competitive interactions.** The spectrofluorimetric competitive binding studies were carried out utilizing the fluorescent probes; RB and EB to learn more about how CT-DNA binds to PLB. Both EB and RB exhibit a considerable increase in fluorescence intensity upon binding to DNA<sup>49,50</sup>. It was found that RB attaches in the minor groove of DNA with a predilection for AT-rich regions, whereas EB attaches to DNA via intercalation, according to previously published studies<sup>51,52</sup>. After numerous trials, it was observed that adding PLB to the CT-DNA-EB complex did not almost affect the complex fluorescence intensity. The RB-CT-DNA complex fluorescence intensity reduced as PLB concentration increased (Fig. 4). Consequently, this proves that PLB and RB have a competitive binding relationship on CT-DNA, whereas PLB and EB do not have a competitive binding interaction. These results also support that PLB has a minor groove binding mechanism with CT-DNA instead of intercalation.

**Effect of ionic strength.** As is well known, the ionic strength of the reaction medium affects the intensity of electrostatic interaction significantly. Hence, under physiological settings, the electrostatic force is relatively weak and acts as an auxiliary force in the interaction between ligands and macromolecules<sup>53</sup>. The impact of changing the concentration of NaCl on the binding contact between CT-DNA and PLB was investigated to find out the

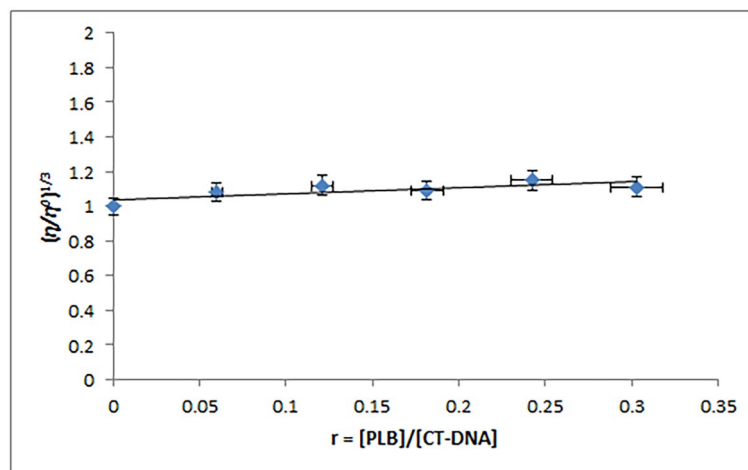


**Figure 3.** Influence of variable concentrations of PLB (0–25.0  $\mu\text{M}$ ) on the viscosity of CT-DNA (82.5  $\mu\text{M}$ ) in Tris-HCl buffer.

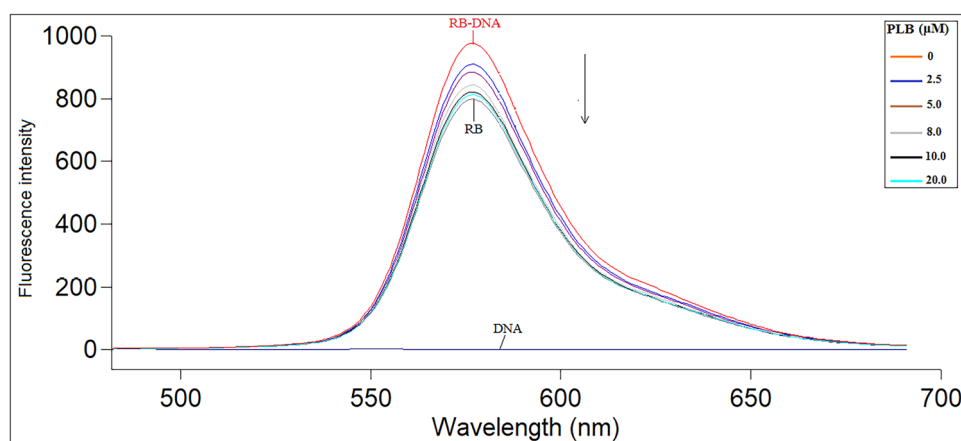


**Figure 4.** Fluorescence emission spectra of RB-CT-DNA complex at 298 K with or without PLB. C(CT-DNA): 57.0  $\mu\text{M}$ ; C(RB): 4.0  $\mu\text{M}$ ; C(PLB) (0–20.0  $\mu\text{M}$ ), ( $\lambda_{\text{ex.}}/\lambda_{\text{em.}} = 465/576 \text{ nm}$ ).

probability of electrostatic interaction between them. The CT-DNA-PLB complex's absorbance value remained relatively constant as the concentration of NaCl was increased from 0 to 0.07 M, as presented in Fig. 5, indicating the absence of electrostatic interaction.

Overall, PLB and CT-DNA showed a minor groove binding interaction, according to the previously described experimental data.

**Evaluation of binding affinity between PLB and CT-DNA.** Since the potency of a drug is directly connected to its binding affinity, studying the drug's binding affinity to a biomacromolecule is critical. The binding constant ( $K_b$ ) or dissociation constant ( $K_d$ ) could be used to determine the binding affinity. The  $K_b$  value of the 1:1 PLB-CT-DNA complex could be calculated by applying the Benesi-Hildebrand Eq. (1)<sup>13,45</sup>:

$$\frac{A_0}{A - A_0} = \frac{\varepsilon_{\text{DNA}}}{\varepsilon_{\text{PLB-DNA}} - \varepsilon_{\text{DNA}}} + \frac{\varepsilon_{\text{DNA}}}{\varepsilon_{\text{PLB-DNA}} - \varepsilon_{\text{DNA}}} \times \frac{1}{K_b \cdot C_{\text{PLB}}} \quad (1)$$

where,  $A$  and  $A_0$  represent CT-DNA absorbance with and without PLB, respectively.  $\varepsilon_{\text{DNA}}$  and  $\varepsilon_{\text{PLB-DNA}}$  are CT-DNA and PLB-CT-DNA complex molar extinction coefficients, respectively.  $C_{\text{PLB}}$  is the PLB concentration.

As shown in Fig. 6,  $1/C_{\text{PLB}}$  was plotted against  $A_0/(A - A_0)$  at each temperature (298, 303, 308, and 313 K). A linear correlation was found, indicating that the PLB-CT-DNA complex has a 1:1 stoichiometry. The  $K_b$  values for the PLB-CT-DNA complex were determined using Eq. (1), and the findings are abridged in Table 2. In the examined range of temperatures, the obtained  $K_b$  values were in the order of  $10^3 \text{ M}^{-1}$ , demonstrating that PLB has a moderate affinity for CT-DNA binding. Furthermore, the  $K_b$  values appear to be in the same range as groove binders<sup>7,10,50,52,54</sup> and lower than those of classic intercalators, as the DNA-EB complex ( $K_b = 1.4 \times 10^6 \text{ M}^{-1}$ )<sup>55,56</sup>, confirming that the binding between PLB and CT-DNA is via a minor groove mechanism.

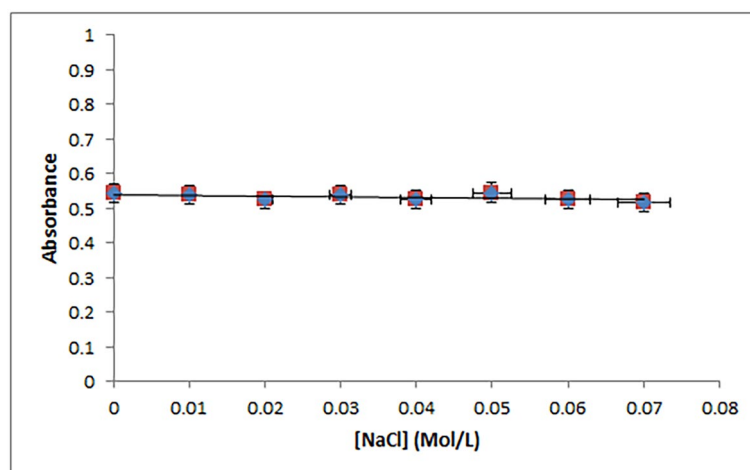


**Figure 5.** Influence of the ionic strength of NaCl on the absorbance of CT-DNA-PLB complex. Concentrations of PLB and CT-DNA were  $2.0 \times 10^{-5}$  M and  $8.25 \times 10^{-5}$  M, respectively. The concentrations of NaCl: 0, 0.01, 0.02, 0.03, 0.04, 0.05, 0.06, 0.07 M.

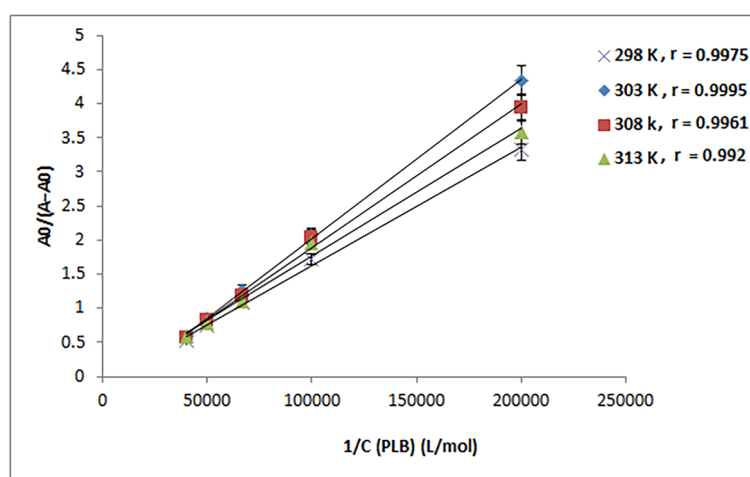


**Figure 6.** Plot of  $A_0/(A-A_0)$  versus  $1/C_{\text{PLB}}$  at different temperature settings ( $C_{\text{DNA}} = 8.25 \times 10^{-5}$  M), where  $r$  is the correlation coefficient.

T (K)	$K_b$ ( $M^{-1}$ )	$r$	S.D	$\Delta H^0$ ( $kJ\ mol^{-1}$ )	$\Delta S^0$ ( $J\ mol^{-1}\ K^{-1}$ )	$\Delta G^{0a}$ ( $kJ\ mol^{-1}$ )	$\Delta G^{0b}$ ( $kJ\ mol^{-1}$ )
298	$6.42 \times 10^3$	0.9975	1.12	-33.09	61.78	-21.72	-21.72
303	$6.26 \times 10^3$	0.9995	1.51			-22.02	-22.03
308	$6.16 \times 10^3$	0.9961	1.36			-22.344	-22.337
313	$6.01 \times 10^3$	0.992	1.23			-22.642	-22.646

**Table 2.** Assessment of the binding constants ( $K_b$ ) at four different temperatures and thermodynamic parameters of the CT-DNA-PLB complex.  $^a \Delta G^0 = RT \ln K_b$ ,  $^b \Delta G^0 = \Delta H^0 - T \Delta S^0$ .

**Assessment of thermodynamic parameters and major interaction forces.** Hydrogen bonding, electrostatic, hydrophobic, and van der Waals forces are four non-covalent binding forces that have been reported to contribute to the binding between biomacromolecules and small molecules<sup>57</sup>. Furthermore, the value and sign of entropy ( $\Delta S^0$ ) and enthalpy ( $\Delta H^0$ ) changes can be used to infer the type of binding forces. When both  $\Delta S^0$  and  $\Delta H^0$  are negative, it is typically assumed that the basic interaction forces are van der Waals force and/or hydrogen bonding. Hydrophobic interaction is the main force when both  $\Delta S^0$  and  $\Delta H^0$  are positive, but electrostatic interaction when  $\Delta S^0$  is positive and  $\Delta H^0$  is approximately zero<sup>26,58</sup>. Van't Hoff Eqs. (2, 3) were

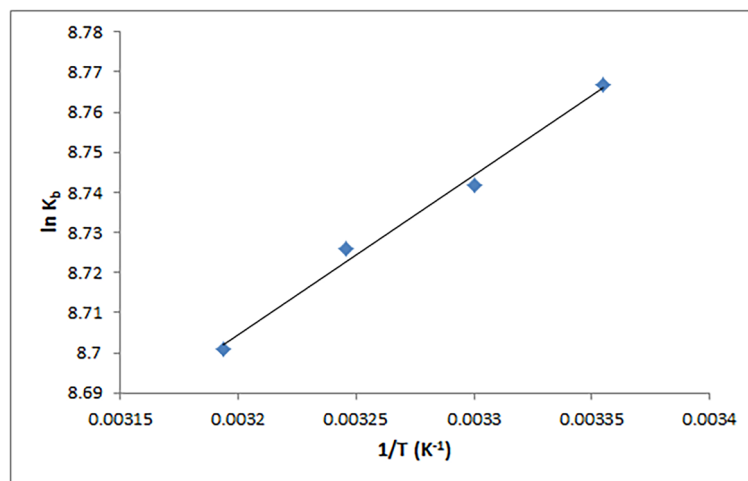


**Figure 7.** Van't Hoff plot for the CT-DNA-PLB complex.

used to determine the thermodynamic parameters in the binding of PLB with CT-DNA, including Gibbs free energy change ( $\Delta G^\circ$ ),  $\Delta S^\circ$ , and  $\Delta H^\circ$ <sup>26</sup>:

$$\ln K_b = -\frac{\Delta H^\circ}{RT} + \frac{\Delta S^\circ}{R} \quad (2)$$

$$\Delta G^\circ = \Delta H^\circ - T\Delta S^\circ \quad (3)$$

where, R represents a gas constant.

$\Delta H^\circ$  and  $\Delta S^\circ$  values were determined using the slope and intercept of the van't Hoff plot of  $\ln K_b$  against  $1/T$  (Fig. 7) and are presented in Table 2. Because  $\Delta G^\circ$  is less than zero, it is concluded that CT-DNA and PLB have a spontaneous binding relationship. The positive  $\Delta S^\circ$  value is commonly because of the hydrophobic interaction. Furthermore, the negative value of  $\Delta H^\circ$  is not an indicator of electrostatic interactions because  $\Delta H^\circ$  is close to zero in the case of electrostatic interactions, implying that the negative  $\Delta H^\circ$  value is likely due to hydrogen bonding interactions<sup>7,50,58–60</sup>. As a result, hydrophobic interactions and hydrogen bonding may be the primary binding forces for the PLB-CT-DNA interaction, as validated by molecular docking studies.

**Determination of conformational changes of CT-DNA.** The conformational changes in the structure of DNA upon the binding interaction with the drugs or other small molecules could be assessed using FT-IR or circular dichroism (CD)<sup>61–65</sup>. Since FT-IR is non-destructive, requires little to no sample preparation, and provides information on all conformations present in the sample, it is an ideal technique for such studies<sup>32</sup>. The spectral characteristics of PLB-CT-DNA complexes are represented in Fig. 8. The region of interest lies in the spectral range 1800–700  $\text{cm}^{-1}$ , which is characterized by deoxyribose stretching of the DNA backbone, nitrogenous base ring vibrations, and  $\text{PO}_2$  stretching vibrations. The vibrational bands at 1711, 1665, 1608, and 1491  $\text{cm}^{-1}$  are ascribed to the nitrogenous bases guanine (G), thymine (T), adenine (A), and cytosine (C), respectively. Bands at 1225 and 1085  $\text{cm}^{-1}$  represent the symmetric and asymmetric phosphate vibrations, respectively<sup>32,66</sup>. These are the distinctive bands of pure CT-DNA examined in this study during the interaction of PLB with CT-DNA at different ratios, and the changes are illustrated in Fig. 8. After adding PLB to the CT-DNA solution, G, T, A, and C bands were observed to exhibit spectral shifts. However, the AT base pairs showed more shifting than GC base pairs which could be clarified by the fitting of PLB into the AT-rich region of the B-DNA minor groove, which is matched with the results of the molecular docking. No significant shifting is observed for phosphate vibrations. These results provide additional evidence that PLB binds to CT-DNA through direct interaction with CT-DNA nitrogenous bases (G, T, A, and C), while CT-DNA remains in the B-conformation<sup>32,63</sup>.

**Molecular modelling.** Using AutoDock 4.2 software, a molecular docking study was performed to elucidate PLB's binding mechanism and elaborate the involved binding forces using three B-DNA sequences (1D29, 3EY0, 1BNA) with a well-studied structure which were used by many research groups for observing the location of the bound probe in CT-DNA<sup>11,13,14,20,50,65,67</sup>. PLB was manipulated as a flexible molecule with five active torsion positions when docked into the B-DNA fragments. With a four-base pair long binding site, PLB exhibited a preference for the AT-rich area of the B-DNA minor groove, as indicated by molecular docking studies (Fig. 9), and the predominant interaction was owing to hydrophobic interactions and hydrogen bonding, which agrees with competitive fluorescence probe assays and UV spectrophotometric measurements. The electrostatic energy (E3) could be excluded from PLB binding forces with DNA fragments when compared to the sum of energies created by other forces (E2), as shown in Table 3. Figure 9 also shows the hydrophobic interaction and hydrogen bonding in the three PLB-DNA complexes. PLB and the DNA basic groups formed three hydrogen bonds and multiple hydrophobic contacts in the PLB-DNA (1BNA and 3EY0) complex. Apart from the hydrophobic contacts in the

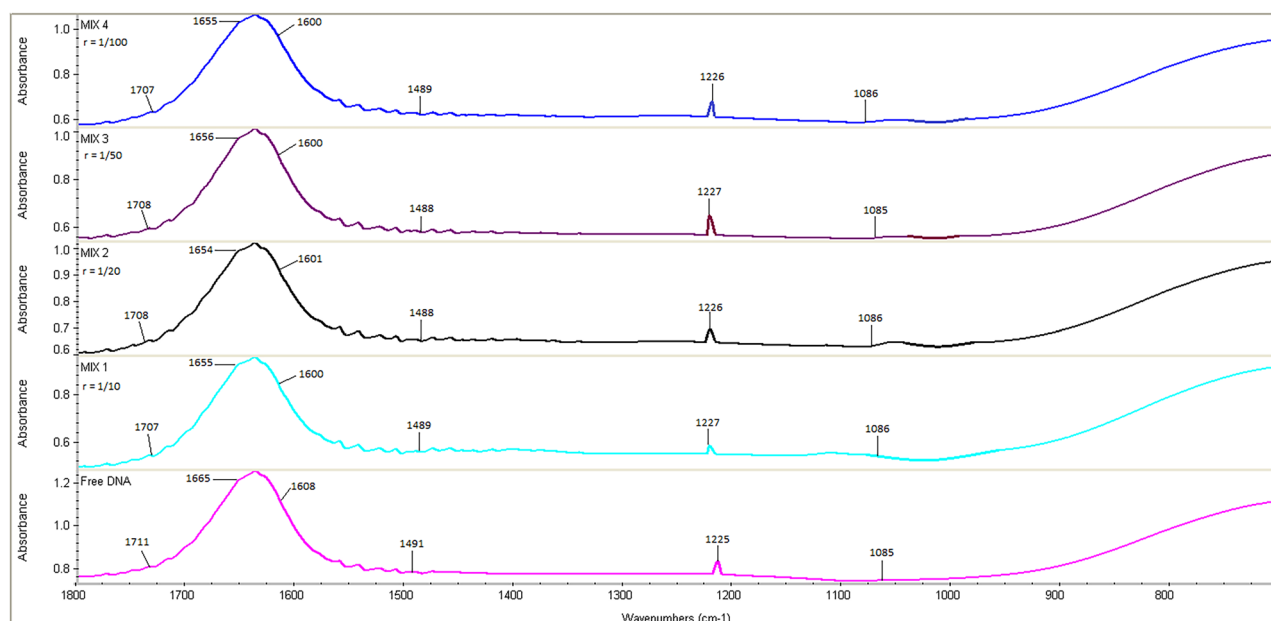


**Figure 8.** Stacked view of FT-IR spectra of free CT-DNA and PLB/CT-DNA ratios of 1/10, 1/20, 1/50, and 1/100 in the region of 1800–700  $\text{cm}^{-1}$ .

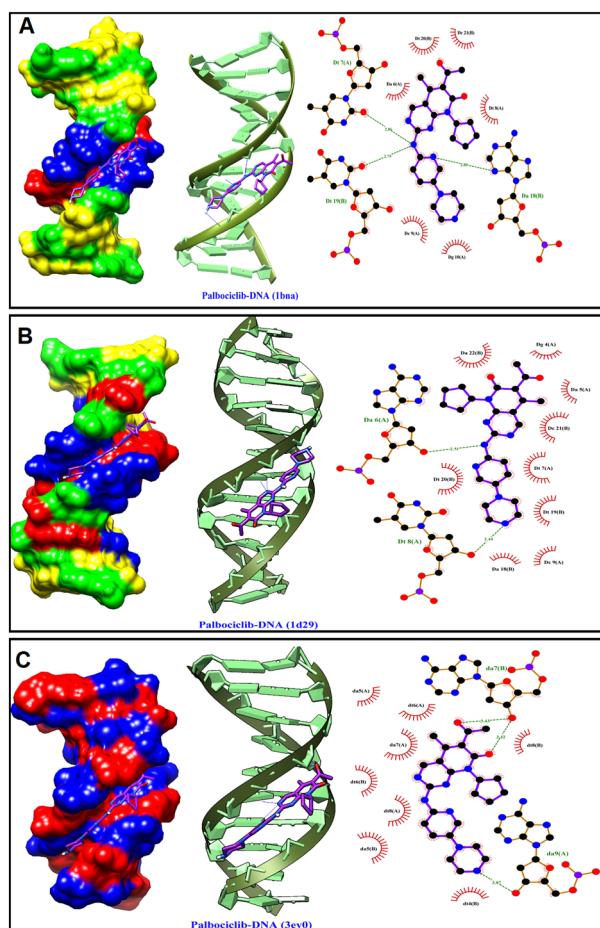


**Figure 9.** The lowest binding free energy pose for PLB on the three B-DNA fragments: Surface view (left) and 2D schematic view (right); deoxy cytosine (DC) is green, deoxy adenine (DA) is red, deoxy guanine (DG) is yellow, deoxy thymine (DT) is blue, cartoon presentation (right), H-bond interactions (green-dashed lines), hydrogen bond length ( $\text{\AA}$ ), and the hydrophobic interactions (red-rays).

PLB-DNA complex	$\Delta G^a$	$E_1^b$	$E_2^c$	$E_3^d$
3EY0	-12.88	-14.37	-11.49	-2.88
1D29	-11.62	-13.11	-10.49	-2.62
1BNA	-11.75	-13.24	-10.07	-3.17

**Table 3.** The different binding energies (Kcal mol<sup>-1</sup>) participated in PLB-DNA complexes. <sup>a</sup> $\Delta G$ : The binding free energy determined in water by the scoring function. <sup>b</sup> $E_1$ : The intermolecular interaction energy, equals the sum of hydrogen bonding energy, van der Waals energy, electrostatic energy, and de-solvation free energy. <sup>c</sup> $E_2$ : The sum of hydrogen bonding, van der Waals, and de-solvation free energies. <sup>d</sup> $E_3$ : The electrostatic energy.

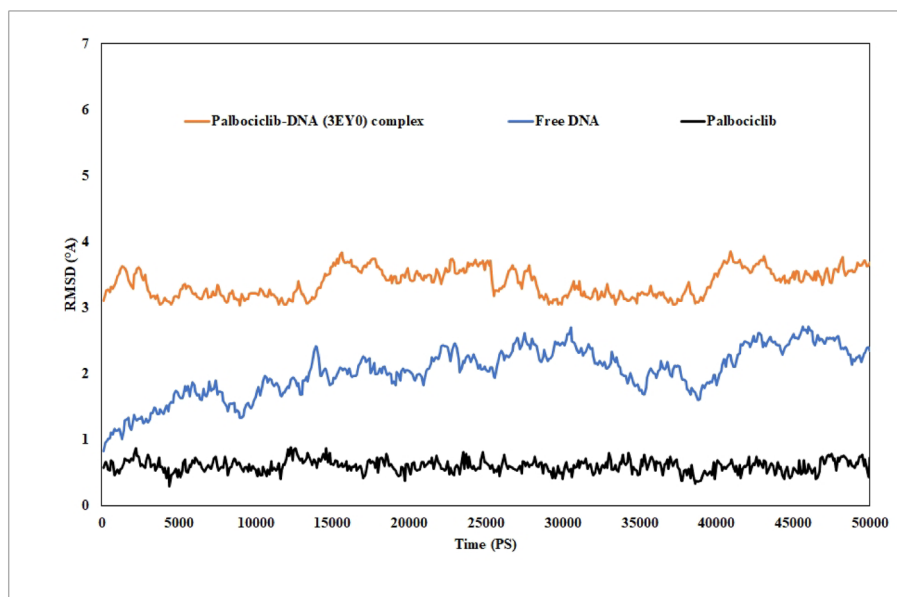


**Figure 10.** RMSD curves for the heavy atoms of free DNA (3EY0) (blue curve), its complex with PLB (orange curve), and free PLB (black curve) after 50 ns dynamic simulation experiments.

minor groove area, PLB and DNA fragment (1D29) had two hydrogen bonding interactions. These findings were consistent with those of the thermodynamic study.

**Molecular dynamic simulation.** An MD simulation study was conducted under physiologically mimic conditions to evaluate the stability and dynamic performance of the PLB-DNA (3EY0) complex, with the root mean square deviation (RMSD), a radius of gyration (Rg), and root mean square fluctuation (RMSF) computed by VMD and presented in Figs. 10, 11, and 12, respectively.

Following the initial 15 ns simulation, the RMSD curve (Fig. 10) for the heavy atoms of free DNA and the PLB-DNA complex revealed to some extent a plateau with a difference of less than 1 Å, indicating that the system has been well equilibrated. Furthermore, the RMSD values of the free PLB heavy atoms showed high stability during the 50 ns simulation, demonstrating that the compound remained bound during the entire simulation time.

Rg is considered a measure of DNA compactness; accordingly, Rg measurements can provide information about changes in DNA structure and thus its structural stability<sup>7,41,68</sup>. Figure 11 demonstrates that during the MD simulation, the Rg values for free DNA and the DNA-PLB complex were nearly comparable with a difference of less than 1 Å, indicating that when PLB attached to DNA did not induce any conformational changes, which was consistent with the results of the FT-IR spectroscopy.

The RMSF results (Fig. 12) showed that no significant fluctuation occurred in nearly all atoms of the bound DNA except for the DNA terminals that are remote from the PLB binding region. This is clearly observed from the RMSF values per DNA bases, where the bound DNA values showed nearly typical values of free DNA, and this supports the stability of the formed complex. Moreover, the distance changes over the 50 ns simulation time showed high stability as observed in small changes in the distances of the interacting bases with PLB showing bases thymine(A)6, adenine(A)7 thymine(A)8, adenine(A)9, adenine(B)5, thymine(B)6, adenine(B)7, and thymine(B)8 which were in close contact to the ligand (Fig. 13). Overall, the MD simulation results supported the experimental and docking data, confirming that PLB bound to CT-DNA in a stable manner.

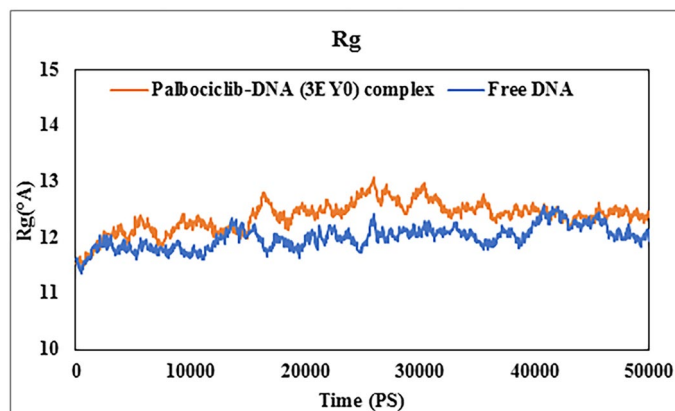


**Figure 11.** Radius of gyration ( $R_g$ ) curves for free DNA (3EY0) (blue curve) and its complex with PLB (orange curve) after 50 ns dynamic simulation experiments.

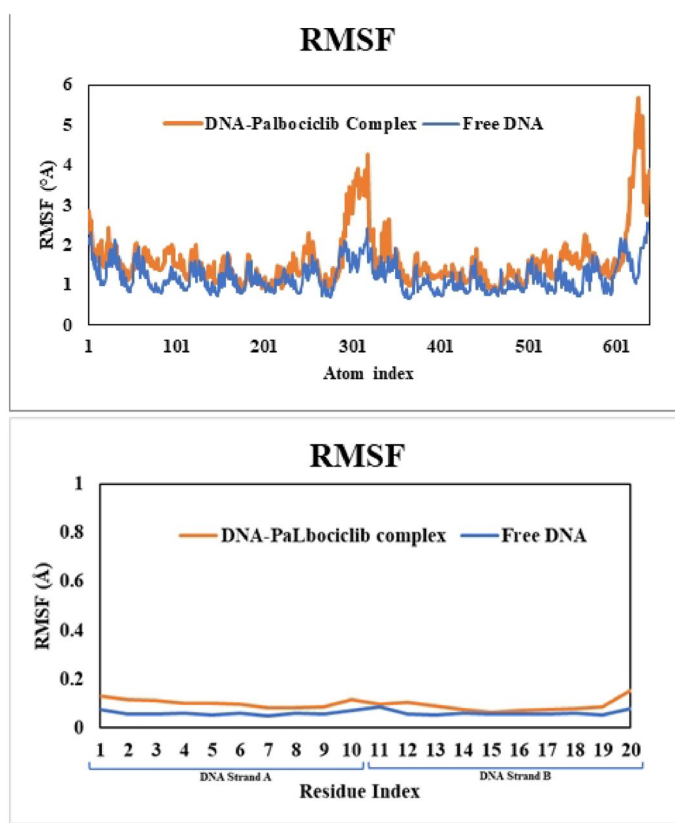


**Figure 12.** RMSF curves for free DNA (3EY0) (blue curve) and its complex with PLB (orange curve) after 50 ns dynamic simulation experiments per atom (Top) and DNA bases (Bottom) for strand A (atom 1–319, residue 1–10) and strand B (atom 320–638, residue 11–20).

## Conclusion

The *in vitro* molecular binding experiments have a substantial advantage that allows a precise assessment of the interaction between small molecules and DNA. The current work introduces the first study of the binding interaction of PLB with CT-DNA by applying several spectroscopic and *in silico* approaches. Through the examination of UV–Vis absorption and viscosity measurements, the complex formation between PLB and CT-DNA has been confirmed via a minor groove binding manner. The calculated binding constant was in the range of  $10^3 \text{ M}^{-1}$ , which is in the same range of familiar groove binders, confirming the moderate binding affinity. Competitive spectrofluorimetric displacement studies using RB and EB revealed that PLB interacts with CT-DNA through groove binding rather than intercalation. The conformational changes of CT-DNA structure in the binding interaction with PLB were also studied using FT-IR spectroscopy. Evaluation of the thermodynamic parameters

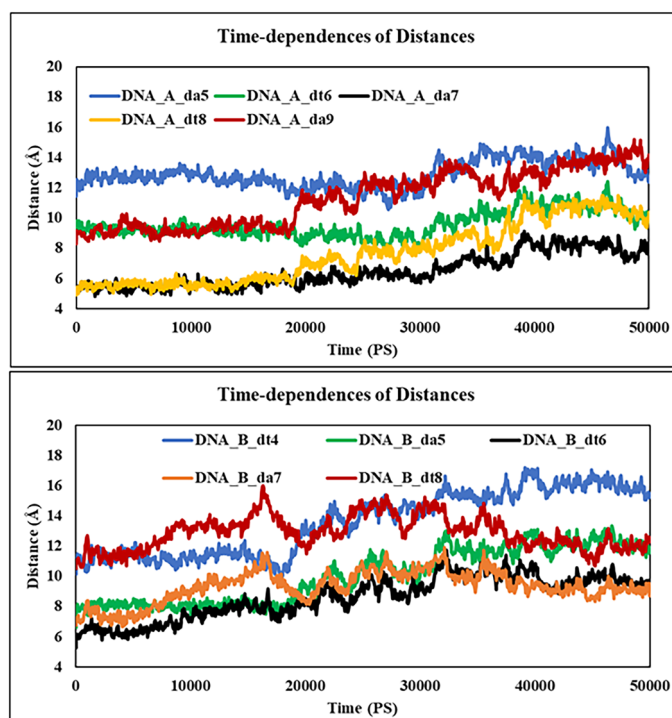


**Figure 13.** Time-dependence of distances for the center of masses of DNA bases with PLB showing the important interacting bases of strand A (Top) and strand B (Bottom).

revealed that PLB's binding to CT-DNA was spontaneous, and hydrogen bonding and hydrophobic interactions were the primary binding forces that stabilized the CT-DNA-PLB complex. The experimental results were further confirmed by the molecular docking and molecular dynamic simulation studies. Overall, this research offered detailed information about the nature of this interaction, including binding mode, binding constant, specific binding site, and interaction forces which are worthwhile for the rational drug scheming with enhanced or more selective activity and greater efficacy.

### Data availability

The datasets generated and/or analyzed during the current study are available from the corresponding author on reasonable request.

Received: 21 June 2022; Accepted: 23 August 2022

Published online: 30 August 2022

### References

1. National Center for Biotechnology Information. PubChem Compound Summary for CID 5330286, Palbociclib. <https://pubchem.ncbi.nlm.nih.gov/compound/Palbociclib>. Accessed 18 February 2022.
2. Center for drug evaluation and research. 207103Orig1s000 (2022).
3. Liu, M., Liu, H. & Chen, J. Mechanisms of the CDK4/6 inhibitor palbociclib (PD 0332991) and its future application in cancer treatment. *Oncol. Rep.* **39**, 901–911 (2018).
4. MedlinePlus, National Library of Medicine (US) (2022).
5. Serra, F. *et al.* Palbociclib in metastatic breast cancer: Current evidence and real-life data. *Drugs Context* **8**, 212579 (2019).
6. Zhang, D., Pan, J., Gong, D. & Zhang, G. Groove binding of indole-3-butyric acid to calf thymus DNA: Spectroscopic and in silico approaches. *J. Mol. Liq.* **347**, 118323 (2022).
7. Magdy, G., Belal, F., Hakiem, A. F. A. & Abdel-Megied, A. M. Salmon sperm DNA binding study to cabozantinib, a tyrosine kinase inhibitor: Multi-spectroscopic and molecular docking approaches. *Int. J. Biol. Macromol.* **182**, 1852–1862 (2021).
8. Huang, G., Ma, J., Li, J. & Yan, L. Study on the interaction between aflatoxin M1 and DNA and its application in the removal of aflatoxin M1. *J. Mol. Liq.* **355**, 118938 (2022).
9. Chen, Q.-Y. *et al.* Interaction of a novel red-region fluorescent probe, Nile Blue, with DNA and its application to nucleic acids assay. *Analyst* **124**, 901–906 (1999).
10. Shahabadi, N. & Hadidi, S. Spectroscopic studies on the interaction of calf thymus DNA with the drug levetiracetam. *Spectrochim. Acta A.* **96**, 278–283 (2012).
11. Luo, Y.-J. *et al.* Assessment on the binding characteristics of dasatinib, a tyrosine kinase inhibitor to calf thymus DNA: Insights from multi-spectroscopic methodologies and molecular docking as well as DFT calculation. *J. Biomol. Struct. Dyn.* **38**, 4210–4220 (2020).
12. Kou, S.-B. *et al.* Investigation of binding characteristics of ritonavir with calf thymus DNA with the help of spectroscopic techniques and molecular simulation. *J. Biomol. Struct. Dyn.* **40**, 2908–2916 (2022).

13. Chen, K.-Y., Zhou, K.-L., Lou, Y.-Y. & Shi, J.-H. Exploring the binding interaction of calf thymus DNA with lapatinib, a tyrosine kinase inhibitor: Multi-spectroscopic techniques combined with molecular docking. *J. Biomol. Struct. Dyn.* **37**, 576–583 (2019).
14. Chen, X. J. *et al.* Characterizing the binding interaction between erlotinib and calf thymus DNA in vitro using multi-spectroscopic methodologies and viscosity measurement combined with molecular docking and DFT calculation. *ChemistrySelect* **4**, 3774–3781 (2019).
15. Hussain, I., Fatima, S., Siddiqui, S., Ahmed, S. & Tabish, M. Exploring the binding mechanism of  $\beta$ -resorcylic acid with calf thymus DNA: Insights from multi-spectroscopic, thermodynamic and bioinformatics approaches. *Spectrochim. Acta A* **260**, 119952 (2021).
16. Sohrabi, T., Hosseinzadeh, M., Beigoli, S., Saberi, M. R. & Chamani, J. Probing the binding of lomefloxacin to a calf thymus DNA-histone H1 complex by multi-spectroscopic and molecular modeling techniques. *J. Mol. Liq.* **256**, 127–138 (2018).
17. Jin, L. *et al.* Study on the interaction between cinnamic acid and DNA with spectroscopy and molecular docking technique. *J. Mol. Liq.* **341**, 117357 (2021).
18. Pathak, M. *et al.* Binding of ethyl pyruvate to bovine serum albumin: Calorimetric, spectroscopic and molecular docking studies. *Thermochim. Acta* **633**, 140–148 (2016).
19. Siddiqui, S., Ameen, F., Jahan, I., Nayeem, S. M. & Tabish, M. A comprehensive spectroscopic and computational investigation on the binding of the anti-asthmatic drug triamcinolone with serum albumin. *New J. Chem.* **43**, 4137–4151 (2019).
20. Mukherjee, A. *et al.* Molecular recognition of synthesized halogenated chalcone by calf thymus DNA through multispectroscopic studies and analysis the anti-cancer, anti-bacterial activity of the compounds. *J. Mol. Liq.* **337**, 116504 (2021).
21. Mukherjee, A., Mondal, S. & Singh, B. Spectroscopic, electrochemical and molecular docking study of the binding interaction of a small molecule 5H-naphtho [2, 1-f][1, 2] oxathieaphine 2, 2-dioxide with calf thymus DNA. *Int. J. Biol. Macromol.* **101**, 527–535 (2017).
22. Mukherjee, A. *et al.* Synthesis, characterization and unravelling the molecular interaction of new bioactive 4-hydroxycoumarin derivative with biopolymer: Insights from spectroscopic and theoretical aspect. *J. Photochem. Photobiol. B* **189**, 124–137 (2018).
23. Nawaz, H., Rauf, S., Akhtar, K. & Khalid, A. M. Electrochemical DNA biosensor for the study of ciprofloxacin–DNA interaction. *Anal. Biochem.* **354**, 28–34 (2006).
24. Shahabadi, N. & Moghadam, N. H. Determining the mode of interaction of calf thymus DNA with the drug sumatriptan using voltammetric and spectroscopic techniques. *Spectrochim. Acta A* **99**, 18–22 (2012).
25. Sarkar, D., Das, P., Basak, S. & Chattopadhyay, N. Binding interaction of cationic phenazinium dyes with calf thymus DNA: A comparative study. *J. Phys. Chem. B* **112**, 9243–9249 (2008).
26. Shi, J.-H., Chen, J., Wang, J. & Zhu, Y.-Y. Binding interaction between sorafenib and calf thymus DNA: spectroscopic methodology, viscosity measurement and molecular docking. *Spectrochim. Acta A* **136**, 443–450 (2015).
27. Shakibapour, N., DehghaniSani, F., Beigoli, S., Sadeghian, H. & Chamani, J. Multi-spectroscopic and molecular modeling studies to reveal the interaction between propyl acridone and calf thymus DNA in the presence of histone H1: Binary and ternary approaches. *J. Biomol. Struct. Dyn.* **37**, 359–371 (2019).
28. Rahman, Y. *et al.* Unravelling the interaction of pirenzepine, a gastrointestinal disorder drug, with calf thymus DNA: An in vitro and molecular modelling study. *Arch. Biochem. Biophys.* **625**, 1–12 (2017).
29. Kumar, C. & Asuncion, E. H. DNA binding studies and site selective fluorescence sensitization of an anthryl probe. *J. Am. Chem. Soc.* **115**, 8547–8553 (1993).
30. Saha, I. & Kumar, G. S. Spectroscopic characterization of the interaction of phenosafranin and safranin O with double stranded, heat denatured and single stranded calf thymus DNA. *J. Fluorescence* **21**, 247–255 (2011).
31. Alex, S. & Dupuis, P. FT-IR and Raman investigation of cadmium binding by DNA. *Inorganica Chim. Acta* **157**, 271–281 (1989).
32. Jangir, D. K., Tyagi, G., Mehrotra, R. & Kundu, S. Carboplatin interaction with calf-thymus DNA: A FTIR spectroscopic approach. *J. Mol. Struct.* **969**, 126–129 (2010).
33. Morris, G. M. *et al.* AutoDock4 and AutoDockTools4: Automated docking with selective receptor flexibility. *J. Comput. Chem.* **30**, 2785–2791 (2009).
34. Larsen, T. A., Kopka, M. L. & Dickerson, R. E. Crystal structure analysis of the B-DNA dodecamer CGTGAATTCACG. *Biochemistry* **30**, 4443–4449 (1991).
35. Moreno, T., Pous, J., Subirana, J. A. & Campos, J. L. Coiled-coil conformation of a pentamidine–DNA complex. *Acta Crystallogr. D* **66**, 251–257 (2010).
36. Drew, H. R. *et al.* Structure of a B-DNA dodecamer: Conformation and dynamics. *Proc. Natl. Acad. Sci.* **78**, 2179–2183 (1981).
37. Singh, U. C. & Kollman, P. A. An approach to computing electrostatic charges for molecules. *J. Comput. Chem.* **5**, 129–145 (1984).
38. Pettersen, E. F. *et al.* UCSF Chimera—A visualization system for exploratory research and analysis. *J. Comput. Chem.* **25**, 1605–1612 (2004).
39. Laskowski, R. A. & Swindells, M. B. *LigPlot+: Multiple Ligand–Protein Interaction Diagrams for Drug Discovery* (ACS Publications, 2011).
40. Humphrey, W., Dalke, A. & Schulten, K. VMD: Visual molecular dynamics. *J. Mol. Graph.* **14**, 33–38 (1996).
41. Abdelaziz, M. A., Shaldam, M., El-Domany, R. A. & Belal, F. Multi-spectroscopic, thermodynamic and molecular dynamic simulation studies for investigation of interaction of dapagliflozin with bovine serum albumin. *Spectrochim. Acta A* **264**, 120298 (2022).
42. Phillips, J. C. *et al.* Scalable molecular dynamics with NAMD. *J. Comput. Chem.* **26**, 1781–1802 (2005).
43. Best, R. B. *et al.* Optimization of the additive CHARMM all-atom protein force field targeting improved sampling of the backbone  $\phi$ ,  $\psi$  and side-chain  $\chi$ 1 and  $\chi$ 2 dihedral angles. *J. Chem. Theory Comput.* **8**, 3257–3273 (2012).
44. Sirajuddin, M., Ali, S. & Badshah, A. Drug–DNA interactions and their study by UV–Visible, fluorescence spectroscopies and cyclic voltametry. *J. Photochem. Photobiol. B* **124**, 1–19 (2013).
45. Shi, J.-H., Liu, T.-T., Jiang, M., Chen, J. & Wang, Q. Characterization of interaction of calf thymus DNA with gefitinib: Spectroscopic methods and molecular docking. *J. Photochem. Photobiol. B* **147**, 47–55 (2015).
46. Palchadhuri, R. & Hergenrother, P. J. DNA as a target for anticancer compounds: Methods to determine the mode of binding and the mechanism of action. *Curr. Opin. Biotechnol.* **18**, 497–503 (2007).
47. Grueso, E., López-Pérez, G., Castellano, M. & Prado-Gotor, R. Thermodynamic and structural study of phenanthroline derivative ruthenium complex/DNA interactions: Probing partial intercalation and binding properties. *J. Inorg. Biochem.* **106**, 1–9 (2012).
48. Mahadevan, S. & Palaniandavar, M. Spectroscopic and voltammetric studies on copper complexes of 2, 9-dimethyl-1, 10-phenanthrolines bound to calf thymus DNA. *Inorg. Chem.* **37**, 693–700 (1998).
49. Li, J. & Dong, C. Study on the interaction of morphine chloride with deoxyribonucleic acid by fluorescence method. *Spectrochim. Acta A* **71**, 1938–1943 (2009).
50. Shi, J.-H., Pan, D.-Q., Zhou, K.-L. & Lou, Y.-Y. Exploring the binding interaction between herring sperm DNA and sunitinib: Insights from spectroscopic and molecular docking approaches. *J. Biomol. Struct. Dyn.* **37**, 837–845 (2019).
51. Hegde, A. H., Prashanth, S. & Seetharamappa, J. Interaction of antioxidant flavonoids with calf thymus DNA analyzed by spectroscopic and electrochemical methods. *J. Pharm. Biomed. Anal.* **63**, 40–46 (2012).
52. Islam, M. M. *et al.* Binding of DNA with rhodamine B: Spectroscopic and molecular modeling studies. *Dyes Pigm.* **99**, 412–422 (2013).
53. Sahoo, D., Bhattacharya, P. & Chakravorti, S. Quest for mode of binding of 2-(4-(dimethylamino) styryl)-1-methylpyridinium iodide with calf thymus DNA. *J. Phys. Chem. B* **114**, 2044–2050 (2010).

54. Kashanian, S., Javanmardi, S., Chitsazan, A., Omidfar, K. & Paknejad, M. DNA-binding studies of fluoxetine antidepressant. *DNA Cell Biol.* **31**, 1349–1355 (2012).
55. Olmsted, J. III. & Kearns, D. R. Mechanism of ethidium bromide fluorescence enhancement on binding to nucleic acids. *Biochemistry* **16**, 3647–3654 (1977).
56. Waring, M. Complex formation between ethidium bromide and nucleic acids. *J. Mol. Biol.* **13**, 269–282 (1965).
57. Klotz, I. M. Physicochemical aspects of drug-protein interactions: A general perspective. *Ann. N. Y. Acad. Sci.* **226**, 18–35 (1973).
58. Ross, P. D. & Subramanian, S. Thermodynamics of protein association reactions: Forces contributing to stability. *Biochemistry* **20**, 3096–3102 (1981).
59. Guo, J. *et al.* Interaction study on bovine serum albumin physically binding to silver nanoparticles: Evolution from discrete conjugates to protein coronas. *Appl. Surf. Sci.* **359**, 82–88 (2015).
60. Rehman, S. U. *et al.* Deciphering the interactions between chlorambucil and calf thymus DNA: A multi-spectroscopic and molecular docking study. *Arch. Biochem. Biophys.* **566**, 7–14 (2015).
61. Arakawa, H., Neault, J. & Tajmir-Riahi, H. Silver (I) complexes with DNA and RNA studied by Fourier transform infrared spectroscopy and capillary electrophoresis. *Biophys. J.* **81**, 1580–1587 (2001).
62. Ouameur, A. A. & Tajmir-Riahi, H.-A. Structural analysis of DNA interactions with biogenic polyamines and cobalt (III) hexamine studied by Fourier transform infrared and capillary electrophoresis. *J. Biol. Chem.* **279**, 42041–42054 (2004).
63. Saito, S. T., Silva, G., Pungartnik, C. & Brendel, M. Study of DNA–emodin interaction by FTIR and UV–vis spectroscopy. *J. Photochem. Photobiol. B* **111**, 59–63 (2012).
64. Mukherjee, A., Ghosh, S., Pal, M. & Singh, B. Deciphering the effective sequestration of DNA bounded bioactive small molecule Safranin-O by non-ionic surfactant TX-114 and diminution its cytotoxicity. *J. Mol. Liq.* **289**, 111116 (2019).
65. Mukherjee, A. & Singh, B. Binding interaction of pharmaceutical drug captopril with calf thymus DNA: A multispectroscopic and molecular docking study. *J. Luminescence* **190**, 319–327 (2017).
66. Jangir, D. K., Charak, S., Mehrotra, R. & Kundu, S. FTIR and circular dichroism spectroscopic study of interaction of 5-fluorouracil with DNA. *J. Photochem. Photobiol. B* **105**, 143–148 (2011).
67. Sarwar, T., Rehman, S. U., Husain, M. A., Ishqi, H. M. & Tabish, M. Interaction of coumarin with calf thymus DNA: Deciphering the mode of binding by in vitro studies. *Int. J. Biol. Macromol.* **73**, 9–16 (2015).
68. Arnittali, M., Rissanou, A. N. & Harmandaris, V. Structure of biomolecules through molecular dynamics simulations. *Procedia Comput. Sci.* **156**, 69–78 (2019).

### Author contributions

G.M.: conceptualization, methodology, formal analysis, software, visualization, writing-original draft. M.A.S.: molecular docking, molecular dynamic simulation studies. F.B.: conceptualization, resources, investigation, writing-review and editing. H.E.: conceptualization, data curation, writing-review and editing. All authors approved the manuscript for publication.

### Funding

Open access funding provided by The Science, Technology & Innovation Funding Authority (STDF) in cooperation with The Egyptian Knowledge Bank (EKB).

### Competing interests

The authors declare no competing interests.

### Additional information

**Correspondence** and requests for materials should be addressed to G.M.

**Reprints and permissions information** is available at [www.nature.com/reprints](http://www.nature.com/reprints).

**Publisher's note** Springer Nature remains neutral with regard to jurisdictional claims in published maps and institutional affiliations.



**Open Access** This article is licensed under a Creative Commons Attribution 4.0 International License, which permits use, sharing, adaptation, distribution and reproduction in any medium or format, as long as you give appropriate credit to the original author(s) and the source, provide a link to the Creative Commons licence, and indicate if changes were made. The images or other third party material in this article are included in the article's Creative Commons licence, unless indicated otherwise in a credit line to the material. If material is not included in the article's Creative Commons licence and your intended use is not permitted by statutory regulation or exceeds the permitted use, you will need to obtain permission directly from the copyright holder. To view a copy of this licence, visit <http://creativecommons.org/licenses/by/4.0/>.

© The Author(s) 2022